J Supercond Nov Magn (2010) 23: 545–550
DOI 10.1007/s10948-010-0763-3

ORIGINAL PAPER

Effective Surface Impedance of a High-Temperature Superconducting Film in Semiconductor Plasma Substrate at Mid-infrared Frequency

Chien-Jang Wu · Yao-Li Chen · Tzong-Jer Yang

Received: 20 November 2009 / Accepted: 12 February 2010 / Published online: 25 February 2010

Abstract The effective surface impedance of a high-temperature superconducting thin film on a semiconductor plasma substrate is calculated. Two possible configurations are considered. The first one is a superconducting film deposited on a semi-infinite semiconductor substrate. It is seen that there exists a critical film thickness for the superconductor such that a minimum effective surface resistance is attained. The effective surface resistance is strongly dependent on the high-frequency permittivity of semiconductor plasma. The second will be limited to the more practical case, that is, the semiconductor substrate is of finite thickness. The investigation of substrate resonance in the effective surface resistance shows some fundamental distinctions when a semiconductor plasma substrate is introduced.

Keywords Surface impedance · High-temperature superconductors · Semiconductor plasmas · Impedance transform technique

1 Introduction

It is known that the surface impedance Z_s is an important quantity widely used to study the electronic conduction mechanism for a superconducting material. At microwave frequency the surface impedance is generally expressed as

$$Z_s = R_s + jX_s = \sqrt{\frac{j\omega\mu_0}{\sigma_s}}, \tag{1}$$

where R_s is called the surface resistance and X_s is known as the surface reactance. In (1), σ_s is the complex conductivity of a superconductor, ω is the angular frequency of the radiation, and μ_0 is the free-space permeability. For a typical high-temperature superconductor (HTS) system $YBa_2Cu_3O_{7-x}$ (YBCO), expressions for R_s and X_s can be obtained based on the two-fluid model together with the London electrodynamics, with the results [1]

$$R_s = \frac{1}{2}\omega^2\mu_0^2\sigma_n f_n \lambda_L^3, \tag{2}$$

$$X_s = \omega\mu_0\lambda_L, \tag{3}$$

where σ_n is normal-state conductivity, f_n is the fraction of the normal fluid. It can be seen from (2) and (3) that R_s, which indicates the power dissipation, is mainly contributed by the normal fluid, and X_s is directly proportional to the temperature-dependent London penetration depth λ_L.

Equations (1)–(3) in fact define the intrinsic bulk surface impedance for a superconductor occupying the half space. For a single superconducting thin film with finite thickness in space, the surface impedance is referred to as the intrinsic film surface impedance. For a more practical case, the superconducting film should be deposited on a relevant substrate and hence the whole system becomes a layered structure. In this case, the surface impedance is called the effective surface impedance $Z_{s,\mathrm{eff}}$ which can be directly obtained by making use of the impedance transformation technique.

C.-J. Wu (✉) · Y.-L. Chen
Institute of Electro-Optical Science and Technology, National Taiwan Normal University, Taipei 116, Taiwan
e-mail: jasperwu@ntnu.edu.tw

T.-J. Yang
Department of Electrical Engineering, Chung Hua University, Hsinchu 300, Taiwan

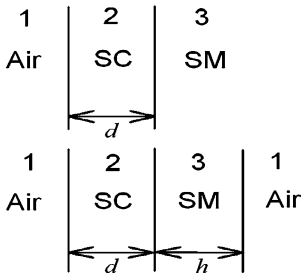

Fig. 1 Two model structures to be considered in this work, where the *top* one is called structure I and the *bottom* one is structure II

There have been many reports on the measurements of effective surface impedances for the familiar HTS systems such as YBCO and $Bi_2Sr_2CaCu_2O_{8-x}$ as well [2–4].

Planar superconducting microwave and photonic devices are mostly fabricated by using YBCO film on a relevant dielectric substrate. The substrates commonly used for YBCO include lanthanum aluminate ($LaAlO_3$), magnesium oxide (MgO) and strontium titanate ($SrTiO_3$). On the other hand, the integration between HTS and semiconductor (SM) has been a perspective in the microelectronics. A successful growth of YBCO film on a semiconducting silicon (Si) substrate has been reported [5]. The effective surface impedance for an YBCO-Si layered structure is also studied, in which the role played by the semiconductor substrate is well illustrated [6]. In addition to Si-substrate the combination of YBCO and resonant semiconductor plasma substrate, $In_{0.53}Ga_{0.47}As$ (IGA) is expected to considerably improve the performances of microwave photonic devices [7].

The purpose of this paper is to theoretically calculate the effective surface impedance at mid-infrared frequency for a layered structure made of YBCO-IGA. IGA provides a convenient material because it has many band-dependent parameters such as the electron effective mass, electron mobility, and high-frequency permittivity. With these parameters, we shall investigate the their effects on the effective surface impedance in a YBCO-IGA structure.

2 Basic Equations

To calculate the effective surface impedance for a high-temperature thin film, two model structures are considered and sketched in Fig. 1, in which the space is divided into regions 1, 2, and 3. Region 1 is the air, the superconductor (SC) is arranged in region 2, and region 3 is occupied by the semiconductor (SM) plasma. The top one is called structure I, where the superconducting film with thickness d is deposited on SM plasma substrate that is assumed to be semi-infinite. The bottom one is referred to as structure II, in which the SM plasma substrate has a finite thickness of h. The effective surface impedance to be calculated in each structure is located at the incident plane boundary, i.e., the interface between layer 1 and 2.

In this study, the SC will be the typical HTS YBCO film. To model the electrodynamics of a high-quality YBCO film, we shall adopt the enhanced two-fluid model reported by Vendik et al. [8]. According to this model, the relative permittivity of YBCO at $T < T_C$ can be expressed as

$$\varepsilon_{r2}(\omega, T) = -\frac{1}{\omega\varepsilon_0}\big[j\sigma_{2,r}(T) + \sigma_{2,i}(\omega, T)\big], \tag{4}$$

where $\sigma_{2,r}(T)$ and $\sigma_{2,i}(\omega, T)$ are the real and imaginary parts of the superconducting complex conductivity, respectively. They are given by

$$\sigma_{2,r}(T) = \sigma_n\left\{\left(\frac{T}{T_C}\right)^{\gamma-1} + \alpha\left[1 - \left(\frac{T}{T_C}\right)^{\gamma}\right]\right\}, \tag{5}$$

$$\sigma_{2,i}(\omega, T) = \frac{1}{\omega\mu_0\lambda_0^2\left[1 - \left(\frac{T}{T_C}\right)^{\gamma}\right]^{-1}}. \tag{6}$$

Here σ_n is the normal-state conductivity of YBCO at $T = T_C$ and λ_0 is the London penetration depth at $T = 0$ K. In addition, α and γ are the empirical parameters. All these parameters, $T_C = 86$ K, $\alpha = 6.5$, $\gamma = 2$, $\lambda_0 = 200$ nm, and $\sigma_n = 10^6$ S/m for YBCO will be used in our next calculation. With the permittivity in (4), the associated wave number in the superconductor is given by

$$k_2 = \omega\sqrt{\mu_0\varepsilon_0\varepsilon_{r2}} = k_0\sqrt{\varepsilon_{r2}}, \tag{7}$$

where $k_0 = \omega\sqrt{\mu_0\varepsilon_0}$ is the free-space wave number. In addition, the intrinsic impedance of a superconductor is written by

$$Z_2 = \sqrt{\frac{\mu_0}{\varepsilon_0\varepsilon_{r2}}} = \frac{Z_0}{\sqrt{\varepsilon_{r2}}}, \tag{8}$$

where $Z_0 = \sqrt{\mu_0/\varepsilon_0} = 120\pi = 377\ \Omega$ is the intrinsic impedance of free space.

As for the semiconductor, we use the resonant semiconductor plasma, IGA, whose relative permittivity is a strong function of frequency at the mid-infrared regime and expressible as [9]

$$\varepsilon_{r3}(\omega) = \varepsilon_\infty\left[1 - \frac{\omega_p^2}{\omega^2}\frac{1}{1 - j\frac{\omega_a}{\omega}}\right], \tag{9}$$

where the plasma frequency is

$$\omega_p = \sqrt{\frac{q^2N}{m^*\varepsilon_\infty\varepsilon_0}}, \tag{10}$$

and the absorption frequency is

$$\omega_a = \frac{q}{m^*\mu_e}, \tag{11}$$

where N is the electron density, m^* is the optical effective mass, μ_e is the electron mobility, q is the absolute value of the electron charge, and ε_∞ is the high-frequency relative permittivity of the bulk material. The wave number and intrinsic impedance of the semiconductor are similarly expressed as in (7) and (8) with a simple replacement of $2 \to 3$.

The effective surface impedance $Z_{s,\mathrm{eff}}$ for structure I can be calculated from the impedance transformation technique, i.e.,

$$Z_{s,\mathrm{eff}}(\omega, T, d) = R_{s,\mathrm{eff}}(\omega, T, d) + jX_{s,\mathrm{eff}}(\omega, T, d) = Z_2 \frac{Z_3 + Z_2 \tanh(jk_2 d)}{Z_2 + Z_3 \tanh(jk_2 d)}. \quad (12)$$

Similarly, the effective surface impedance $Z_{s,\mathrm{eff}}$ for structure II can be obtained by successive impedance transformation. First, the impedance at the interface of superconductor/semiconductor is expressed as

$$Z_{\mathrm{sc/sm}}(\omega, h) = Z_3 \frac{Z_1 + Z_3 \tanh(jk_3 h)}{Z_3 + Z_1 \tanh(jk_3 h)}, \quad (13)$$

where the impedance Z_1 is equal to Z_0. Next, the effective surface impedance of the entire system calculated at the incident plane boundary of air/superconductor is given by

$$Z_{s,\mathrm{eff}}(\omega, T, d, h) = R_{s,\mathrm{eff}}(\omega, T, d, h) + jX_{s,\mathrm{eff}}(\omega, T, d, h) = Z_2 \frac{Z_{\mathrm{sc/sm}} + Z_2 \tanh(jk_2 d)}{Z_2 + Z_{\mathrm{sc/sm}} \tanh(jk_2 d)}. \quad (14)$$

With $Z_{\mathrm{sc/sm}}(\omega, h)$ given in (13), it is seen that $Z_{s,\mathrm{eff}}(\omega, T, d, h)$ expressed in (14) incorporates all possible material parameters, including the intrinsic permittivities and the extrinsic thicknesses as well.

3 Numerical Results and Discussion

3.1 Structure I

In Fig. 2 we plot (a) the effective surface resistance $R_{s,\mathrm{eff}}$ and (b) the effective surface reactance $X_{s,\mathrm{eff}}$ as a function of the wavelength of electromagnetic radiation for structure I at 77 K for five thicknesses of YBCO, $d = 0.1\lambda_0$, $0.5\lambda_0$, λ_0, $2\lambda_0$, and $10\lambda_0$ (corresponding to the curves 1–5, respectively). The material parameters for the semiconductor plasma IGA are $N = 5 \times 10^{24}\ \mathrm{m}^{-3}$, $m^* = 4.099 \times 10^{-32}$ kg, $\mu_e = 0.2\ \mathrm{m}^2/\mathrm{V{\cdot}s}$, and $\varepsilon_\infty = 11.75$. It is seen that for a thin YBCO film, $d = 0.1\lambda_0$ (curve 1), the surface resistance is larger than those for $d > 0.1\lambda_0$ (curves 2–5). In addition, $R_{s,\mathrm{eff}}$ increases as the wavelength increases for $d = 0.1\lambda_0$, and it slightly decreases with increasing wavelength for the other thicknesses. As for the effective surface reactance $X_{s,\mathrm{eff}}$, it is seen from (b) that, for $d = 0.1\lambda_0$, the variation

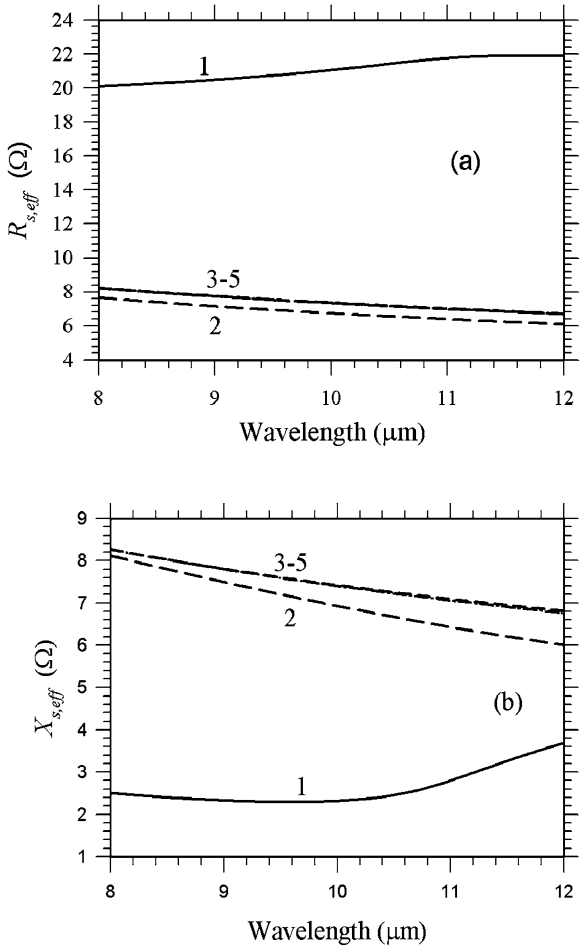

Fig. 2 The calculated wavelength-dependent effective surface resistance $R_{s,\mathrm{eff}}$ (**a**) and effective surface reactance $X_{s,\mathrm{eff}}$ (**b**) at $T = 77$ K for five different thicknesses of YBCO film $d = 0.1\lambda_0, 0.5\lambda_0, \lambda_0, 2\lambda_0$, and $10\lambda_0$ (corresponding to the curves 1–5, respectively) in structure I

in $X_{s,\mathrm{eff}}$ is not large until the wavelength near 10 μm. For wavelength larger than 10 μm, it increases with increasing wavelength. For a thicker film (curves 2–5), $X_{s,\mathrm{eff}}$ monotonically decreases as the wavelength increases.

Figure 3 depicts the effective surface resistance $R_{s,\mathrm{eff}}$ as a function of the thickness of YBCO film at a fixed wavelength of 8 μm for different temperatures, $T = 85$, 80, 77, 4.2 K (curves 1–4, respectively). It is of interest to see that there exists a shallow dip, which enables us to define a critical thickness d_c for YBCO film at which the effective surface resistance attains a minimum. At this critical thickness a minimum in the power loss of the total structure is achieved. This minimum loss is of practical use when the structure is used to be fabricated as a device because the loss issue could determine the device performance. The loss can be substantially increased when the film thickness gets smaller. In addition, this shallow dip is moved to a smaller thickness as the temperature is reduced. In addition, $R_{s,\mathrm{eff}}$ remains nearly a constant when the $d > d_c$, indicating a bulk property of ma-

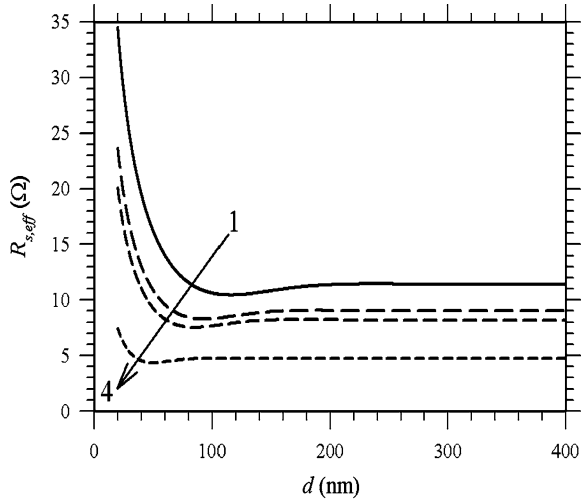

Fig. 3 The calculated effective surface resistance $R_{s,eff}$ as a function of the thickness of YBCO film at a fixed wavelength of 8 μm for distinct temperatures, $T = 85$, 80, 77, and 4.2 K (curves 1–4, respectively) in structure I

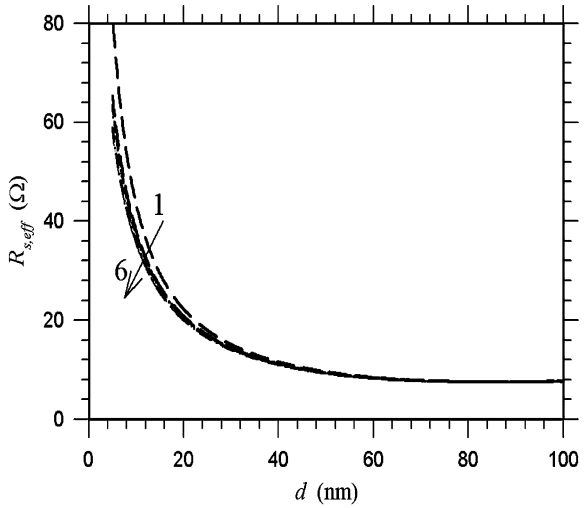

Fig. 5 The thickness-dependent $R_{s,eff}$ for distinct values in high-frequency relative permittivity $\varepsilon_\infty = 6$, 9, 9.6, 10, 11.5, 12 (curves 1–6, respectively) at a fixed wavelength of 8 μm and fixed temperature of 77 K

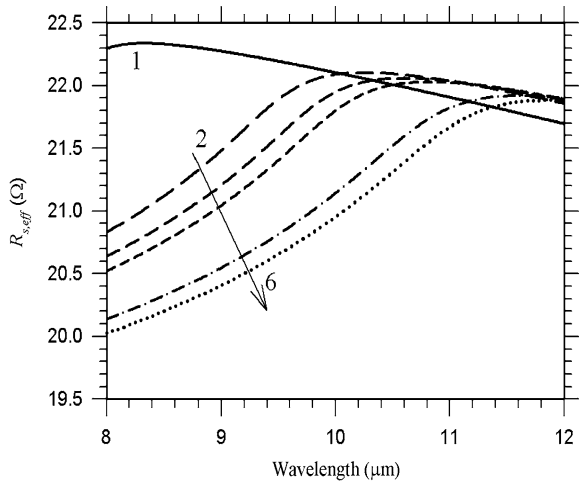

Fig. 4 The calculated wavelength-dependent effective surface resistance for distinct values in high-frequency relative permittivity $\varepsilon_\infty = 6$, 9, 9.6, 10, 11.5, 12 (curves 1–6) for YBCO film with $d = 0.1\lambda_0$ and at temperature $T = 77$ K

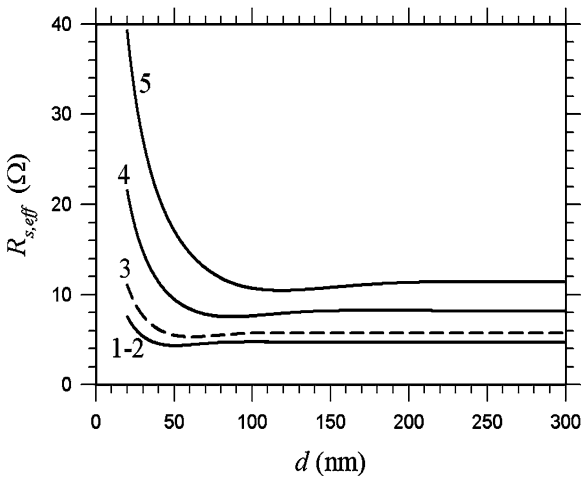

Fig. 6 The calculated effective surface resistance as a function of YBCO thickness for structure II, where the wavelength is 8 μm, and the temperatures are $T = 4.2$, 5.6, 56, 77, and 85 K (curves 1–5, respectively). The IGA material parameters for N, m^*, μ_e, and ε_∞ are 5×10^{24} m^{-3}, 4.099×10^{-32} kg, 0.2 m^2/V·s, and 11.75, respectively

terial. That is, the film properties can be best investigated at a thickness less than the critical thickness. This shallow dip, in fact, does not appear when the substrate is replaced by the usual dielectric material such as MgO, $LaAlO_3$, or $SrTiO_3$.

For the SM plasma, the high-frequency relative permittivity ε_∞ plays an important role in the determination of plasma behavior [9]. Based on this reason, in Fig. 4, we plot the wavelength-dependent effective surface resistance for different values in ε_∞. Three different dependences are seen. First, for $\varepsilon_\infty = 6$ (curve 1), $R_{s,eff}$ generally shows a slow decrease with the increase in the wavelength. Second, for $\varepsilon_\infty = 9, 9.6$, and 10 (curves 2–4), $R_{s,eff}$ increases with increasing wavelength and reaches a maximum around 10 μm for $\varepsilon_\infty = 9$, and then decreases slowly when the wavelength increases. Third, for $\varepsilon_\infty = 11.5$, and 12 (curves 5–6), $R_{s,eff}$ monotonically increases as a function of the wavelength. The results in Fig. 4 illustrate that the wavelength-dependent (or frequency-dependent) surface resistance is strongly affected by the value of the high-frequency permittivity of the semiconductor plasma.

Figure 5 depicts the thickness-dependent $R_{s,eff}$ for various high-frequency relative permittivity $\varepsilon_\infty = 6$, 9, 9.6, 10, 11.5, 12 (curves 1–6, respectively) at a wavelength of 8 μm. The change in ε_∞ does not cause a salient variation in the effective surface resistance.

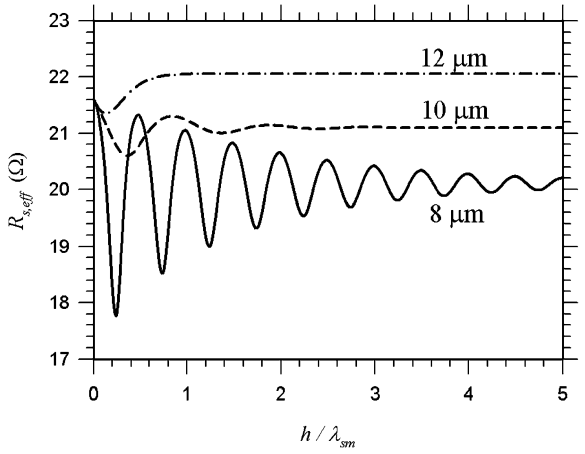

Fig. 7 The calculated effective surface resistance as a function of SM thickness for structure II, where the temperatures are $T = 77$ K, and the wavelength is taken at 8, 10, and 12 μm, respectively. Other material parameters are the same as in Fig. 6

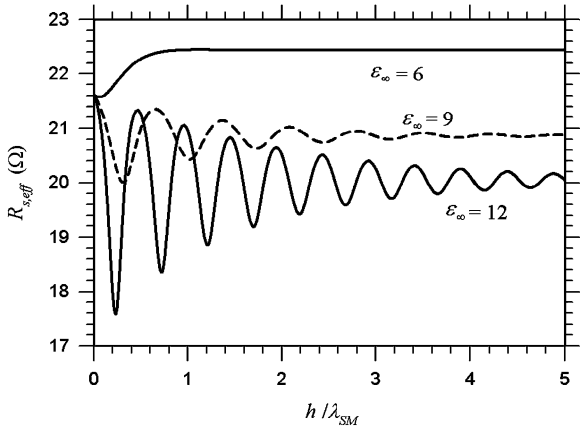

Fig. 8 The calculated $R_{s,eff}$ as a function of λ_{SM}. The relative permittivity of semiconductor plasma IGA is taken as $\varepsilon_\infty = 6$, 9, and 12, respectively

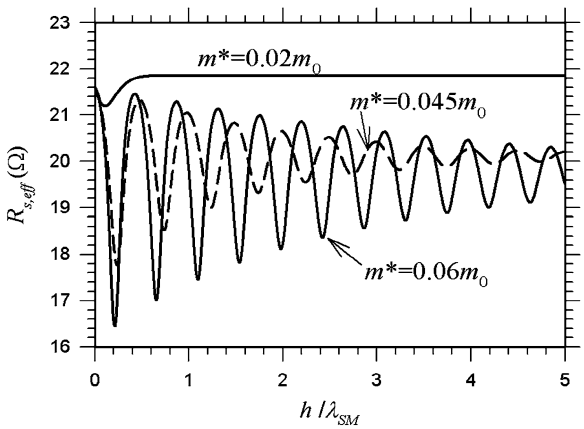

Fig. 9 The calculated $R_{s,eff}$ as a function of the normalized substrate thickness. The wavelength is 8 μm, the relative permittivity of IGA is $\varepsilon_\infty = 11.75$ while the optical electron effective mass is $m^* = 0.02m_0, 0.045m_0, 0.06m_0$, respectively, where $m_0 = 9.1 \times 10^{-31}$ kg is the free electron mass

3.2 Structure II

Let us continue to present the numerical results for structure II. Figure 6 displays the calculated effective surface resistance $R_{s,eff}$ as a function of YBCO film thickness at a wavelength of 8 μm for five temperatures, $T = 4.2$, 5.6, 56, 77, and 85 K (curves 1–5, respectively). The material parameters of IGA are the same as used in Fig. 2. The YBCO film thickness is $d = 20$ nm. The results in Fig. 6 are similar to the case where the substrate is semi-infinite, as depicted in Fig. 3. It should be noted that each curve in Fig. 6 is coincided as one at different thicknesses of SM, i.e., $h = 10$, 20, 50, 100, 200 nm, indicating the variation in $R_{s,eff}$ due to the change in the thickness of IGA substrate is negligible.

Figure 7 shows the calculated effective surface resistance as a function of the normalized SM thickness (normalized to the SM-substrate wavelength λ_{SM}) for three different wavelengths 8, 10, and 12 μm. The SM-substrate wavelength λ_{SM} is defined by $\lambda_{SM} = 2\pi/(\omega\sqrt{\mu_0\varepsilon_0\varepsilon_{r3}})$, which, for these three wavelengths, is calculated to be $\lambda_{SM} = 3.42$, 6.78, and 7.02 mm, respectively. It can be seen that the substrate resonant phenomenon is more salient at 8 μm. The maximum in $R_{s,eff}$ occurs when the SM thickness is equal to an integer multiple of the half substrate wavelength, i.e., $h = n\lambda_{SM}/2$, n = integer. The minimum in $R_{s,eff}$, however, occurs at the condition of $h = n\lambda_{SM}/4$. The oscillation amplitude decreases with increasing substrate thickness. Usually, the substrate resonant phenomenon is seen at $R_{s,eff}$ for a YBCO on common dielectric substrate, where the oscillation amplitude remains constant, not the same as shown in Fig. 7.

Next, we investigate the substrate resonant phenomenon by changing the material parameters for IGA. For different values in the high-frequency relative permittivity ε_∞, in the electron effective mass m^*, and in the electron mobility μ_e, the calculated $R_{s,eff}$ at 77 K and $d = 20$ nm are shown in Figs. 8, 9, and 10, respectively. In Fig. 8 we see that the decrease in the value of ε_∞, the substrate oscillation behavior will disappear at $\varepsilon_\infty = 6$. In Fig. 9, the effect of electron effective mass on the substrate oscillation phenomenon in $R_{s,eff}$ is illustrated, in which three different effective masses are taken. The oscillating behavior is more pronounced at a larger electron effective mass. In addition, the oscillation curve is also shifted due to the variation of the effective mass.

In Fig. 10, we plot the $R_{s,eff}$ versus SM thickness for different mobilities, $\mu_e = 0.01$, 0.1, 0.2, 0.5, and 1.0 $m^2/V{\cdot}s$, respectively. The oscillating amplitude greatly increases with the increase in the mobility. According to (11), the mobility is inversely proportional to the absorption frequency. Thus, a higher mobility indicates less absorption, which in turn leads to a strong oscillation in the effective surface re-

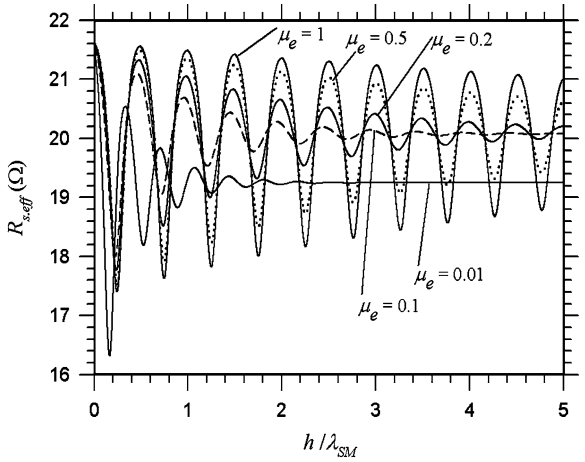

Fig. 10 The calculated $R_{s,eff}$ as a function of the normalized substrate thickness. The wavelength is 8 μm and its substrate wavelength is $\lambda_{SM} = 3.421$ μm. The relative permittivity of IGA is $\varepsilon_\infty = 11.75$, the optical electron effective mass is $m^* = 4.099 \times 10^{-32}$ kg, and the electron mobility is taken to be $\mu_e = 0.01$, 0.1, 0.2, 0.5, and 1.0 $m^2/V{\cdot}s$, respectively

sistance. At a lower mobility, the loss will be considerably enhanced such that the oscillating behavior is strongly depressed.

4 Conclusion

The effective surface impedance of a layered structure made of YBCO and IGA is theoretically calculated and investigated. Two model structures are used to study the surface impedance in this work. For structure I, the effective surface resistance defines a critical YBCO-film thickness at which a minimum loss is attained. In addition, this critical thickness can be characterized as the boundary for the thin film and bulk properties. In the structure, we illustrate the substrate resonance behavior due to the IGA substrate. With a strongly dispersive in the permittivity for IGA, the substrate resonance is obviously different from that of in the usual dielectric substrates for YBCO.

Acknowledgements C.-J. Wu acknowledges the financial support from the National Science Council of the Republic of China (Taiwan) under Contract No. NSC-97-2112-M-003-013-MY3.

References

1. Duzer, T.V., Turner, C.W.: Principle of Superconductive Devices and Circuits. Elsevier, New York (1981)
2. Trunin, M.R.: J. Supercond. **11**, 381 (1998)
3. Newman, N., Lyons, W.G.: J. Supercond. **6**, 119 (1993)
4. Gollop, J.: Supercond. Sci. Technol. **10**, A120 (1997)
5. Mechin, L., Villegier, J.-C., Rolland, G., Laugier, F.: Physica C **269**, 124 (1996)
6. Pompeo, N., Marcon, R., Silva, E.: J. Supercond. Nov. Magn. **19**, 611 (2006)
7. Hamada, M.S., Shabat, M.M., Elaal Abd, M.M., Jager, D.: J. Supercond. Nov. Magn. **16**, 443 (2003)
8. Vendik, O.G., Vendik, I.B., Kaparkov, D.I.: IEEE Trans. Microw. Theory Technol. **46**, 469 (1998)
9. Stiens, J., Vounckx, R., Veretennicoff, I., Voronko, A., Shkerdin, G.: J. Appl. Phys. **81**, 1 (1997)